BOSTON UNIVERSITY

GRADUATE SCHOOL OF ARTS AND SCIENCES

Dissertation

MEASUREMENT OF THE ANOMALOUS MAGNETIC MOMENT OF THE POSITIVE MUON TO .SOMETHING PARTS PER BILLION

by

NICHOLAS BRENNAN KINNAIRD

B.S., University of Texas at Austin, 2013
B.S., University of Texas at Austin, 2013
M.A., Boston University, 2016

Submitted in partial fulfillment of the

requirements for the degree of

Doctor of Philosophy

2019

Approved by

First Reader

B. L. Roberts, PhD
Professor of Physics

Second Reader

R. M. Carey, PhD
Professor of Physics

Third Reader

J. P. Miller, PhD
Professor of Physics

Dedication

I dedicate this thesis to

Acknowledgments

Here go all your acknowledgments. You know, your advisor, funding agency, lab mates, etc., and of course your family.

As for me, I would like to thank Jonathan Polimeni for cleaning up old LaTeX style files and templates so that Engineering students would not have to suffer typesetting dissertations in MS Word. Also, I would like to thank IDS/ISS group (ECE) and CV/CNS lab graduates for their contributions and tweaks to this scheme over the years (after many frustrations when preparing their final document for BU library). In particular, I would like to thank Limor Martin who has helped with the transition to PDF-only dissertation format (no more printing hardcopies – hooray !!!)

The stylistic and aesthetic conventions implemented in this LaTeX thesis/dissertation format would not have been possible without the help from Brendan McDermot of Mugar library and Martha Wellman of CAS.

Finally, credit is due to Stephen Gildea for the MIT style file off which this current version is based, and Paolo Gaudiano for porting the MIT style to one compatible with BU requirements.

Janusz Konrad

Professor

ECE Department

MEASUREMENT OF THE ANOMALOUS MAGNETIC MOMENT OF THE POSITIVE MUON TO .SOMETHING PARTS PER BILLION

(Order No.)

NICHOLAS BRENNAN KINNAIRD

Boston University, Graduate School of Arts and Sciences, 2019

Major Professor: B. L. Roberts, Professor of Physics

ABSTRACT

Have you ever wondered why this is called an *abstract*? Weird thing is that its legal to cite the abstract of a dissertation alone, apart from the rest of the manuscript.

Contents

List of Tables

List of Figures

List of Abbreviations

ppm	....	parts per million
ppb	....	parts per billion
BNL	....	Brookhaven National Laboratory
FNAL	....	Fermi National Accelerator Laboratory
SM	....	Standard Model
SiPM	....	Silicon Photo-Multiplier
Geane	....	Geometry and Error Propagation
Geant4	....	Geometry and Tracking 4

Chapter 1

Introduction

While the prevailing theory for particle physics, the Standard Model (SM), has had tremendous success in describing our universe, there exist unanswered questions. These namely include the matter-antimatter asymmetry, the source of mass for the neutrinos, the existance of dark matter, and more. Many particle physics experiments are being conducted around the world in order to shed light on these questions and round out our understanding of reality. One such particular experiment being conducted is the Fermilab Muon $g-2$ Experiment (E989) underway at the Fermi National Accelerator Laboratory (FNAL) located in Batavia, Illinois. It has the goal of measuring the magnetic moment of the muon, proportional to the g in $g-2$, to high precision in order to compare to SM theoretical predictions. Because the magnetic moment of particles couple to all existing particles, known or unknown, (source this? reference to a later section?) this provides an avenue through which theories might be constrained, and new physics narrowed down. Indeed this experiment is the latest in a line of such experiments which have measured the magnetic moment of the muon over the past several decades, the last of which measured the magnetic moment of the muon to .54 parts per million (ppm) at Brookhaven National Laboratory (BNL) in 2001 [4].

1.1 Background

The previous $g-2$ experiment at BNL measured a discepancy in the magnetic moment of the muon between theory and experiment with a 2.2 - 2.7 standard deviation. (Cite the final report again?) That disagreement has since grown above 3σ [12], depending on the theoretical analysis approaches used.

1.1.1 Definitions

$$\vec{\mu} = g\frac{Qe}{2m}\vec{s} \tag{1.1}$$

$$a = \frac{g-2}{2} \tag{1.2}$$

-would it be worthwhile to include my derivation on the magnetic moment like in my hep presentation?

1.1.2 Experiment History

-do I want this? I'm sort of already talking about this for E821 in the intro and background - I don't think I want to go into the older experiments

1.2 Theory

Feynamn diagrams made with [6], [5].

1.2.1 QED

1.2.2 Weak

1.2.3 Hadronic

1.2.4 BSM

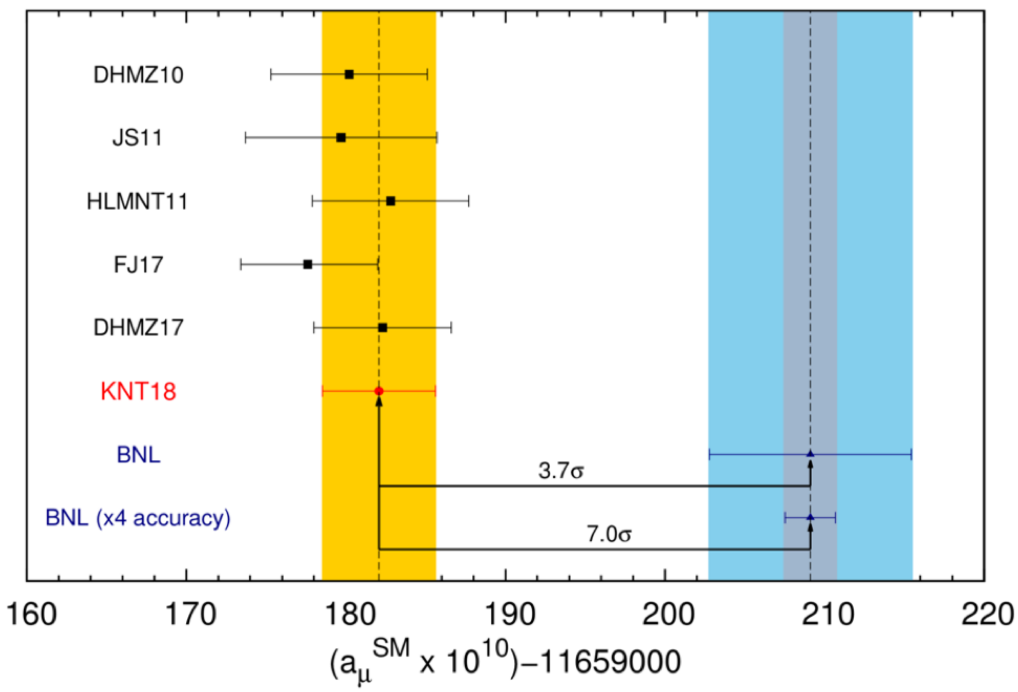

Figure 1·1: clean up and possibly replace

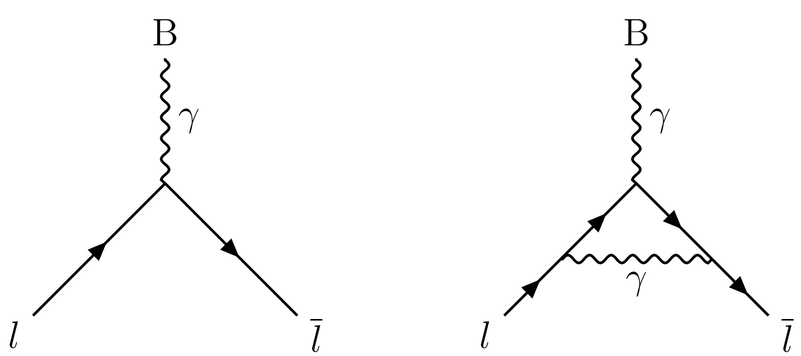

(a) test1

(b) test2

Figure 1·2: clean up and possibly replace - cite this package if I end up using it

Chapter 2

Muon g-2 at Fermilab, E989

2.1 Principle Technique

In a dipole magnetic field, particles will orbit at the cyclotron frequency

$$\omega_c = -\frac{Qe}{\gamma m}B, \tag{2.1}$$

and their spins will turn at the precession frequency

$$\omega_s = -g\frac{Qe}{2m}B - (1-\gamma)\frac{Qe}{\gamma m}B, \tag{2.2}$$

where $Q = \pm 1$ and $e > 0$. The difference between these two frequencies gives

$$\omega_a = \omega_s - \omega_c = -\frac{g-2}{2}\frac{Qe}{m}B = -a\frac{Qe}{m}B, \tag{2.3}$$

a measureable frequency that is directly proportional to the property of significance, the anamoly a. By measuring the spin difference frequency for muons and the magnetic field B, a_μ can be determined. In the presence of an electric field, which is useful in storing the muon beam within a dipole magnetic field, this expands to

$$\vec{\omega}_a = -\frac{Qe}{m}[a_\mu \vec{B} - (a_\mu - \frac{1}{\gamma^2 - 1})(\vec{\beta} \times \vec{E})], \tag{2.4}$$

where now the measurable quanties are vector quantities. Finally, for realistic cases of muon momentum which is non-orthogonal to the magnetic field, the spin difference frequency becomes

$$\vec{\omega}_a = -\frac{Qe}{m}[a_\mu \vec{B} - a_\mu(\frac{\gamma}{\gamma+1})(\vec{\beta}\cdot\vec{B})\vec{B} - (a_\mu - \frac{1}{\gamma^2-1})(\vec{\beta}\times\vec{E})]. \tag{2.5}$$

If the motion of the muons is largely perpendicular to the magnetic field, then the second term is small and can be corrected for. If the particles have a momentum of approximately 3.09 GeV/c, the so called "magic momentum," then the third term is small and can be corrected for. These will be talked about later.

In order to measure the spin difference frequency of the muon, a clever technique is used. Decay muons in the pion rest frame are 100% polarized due to conservation of angular momentum and the fact that the decay neutrino must have a specific helicity. Within a pion beam then the highest and lowest energy decay muons are polarized. Muons will decay to positrons with a lifetime of about 2.2 μs, and the positrons with the highest energies will be correlated with the muon spin, a so called "self-analyzing" decay. The single available decay state for a maximum energy positron illustrates this in Figure ??. Thus, by aquiring a large sample of polarized muons and injecting them into a storage ring

-explain the physics -explain how we get at the physics with our ring and detectors -parity violation -actually write out the decay states before explaining some things - well shouldn't these have been talked about before?? maybe not -decay probabilities and all that -don't measure all decay positrons -By injecting a large ensemble of muons and -by measuring a subset of ensemble of muons.... -Careful with spin vs polarization

2.2 Accelerator

[15]

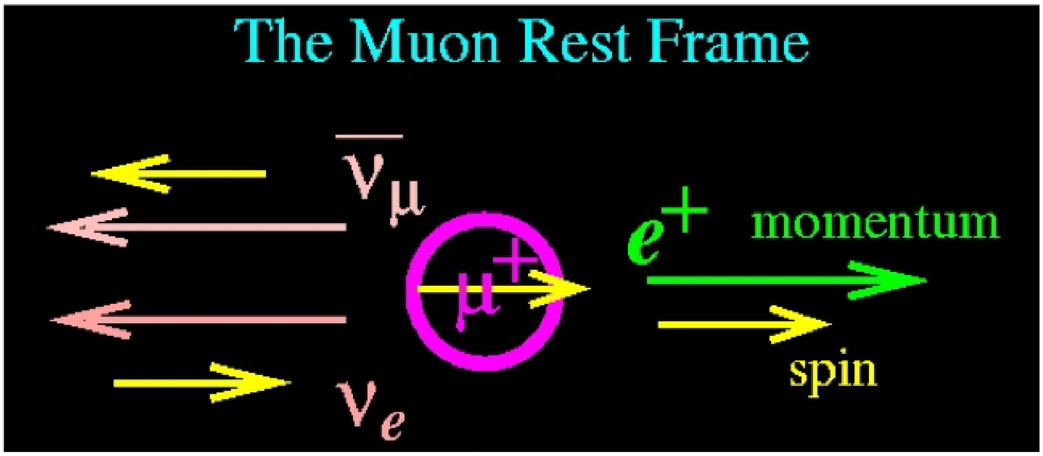

Figure 2·1: Make a new version of this picture, and improve this caption.: The single available decay state for maximum energy decay positrons. Due to the conservation of angular momentum and the single possible helicity states of the decay neutrino and anti-neutrino, the spin of the decay positron is exactly equal to the spin of the muon at the time of the decay.

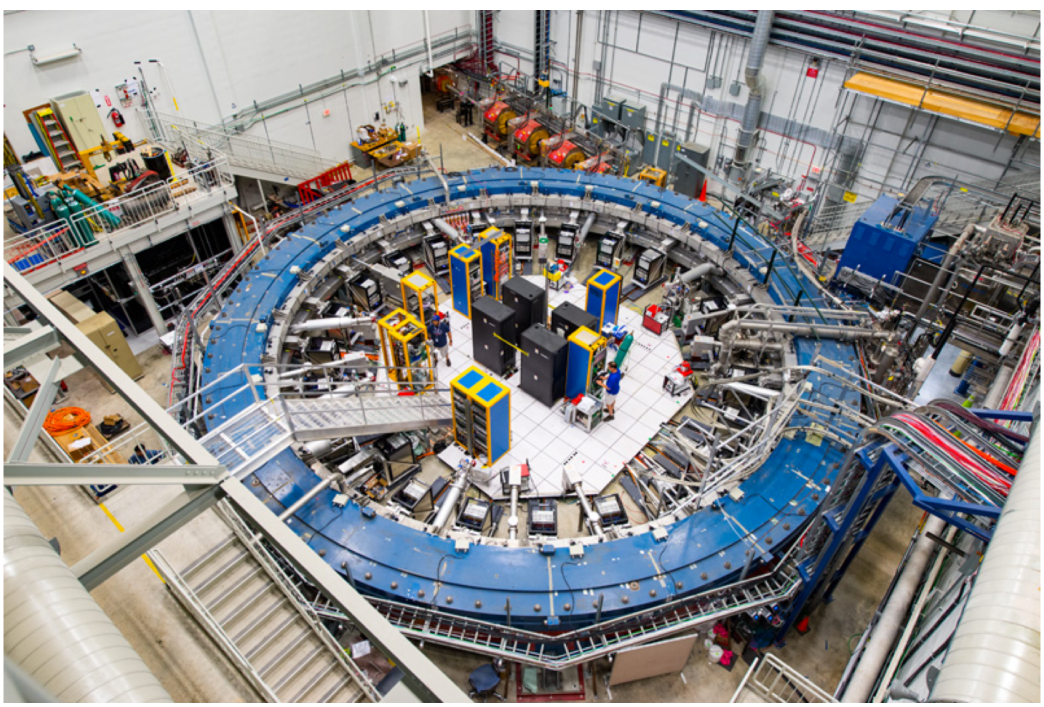

Figure 2·2: clean up and possibly replace

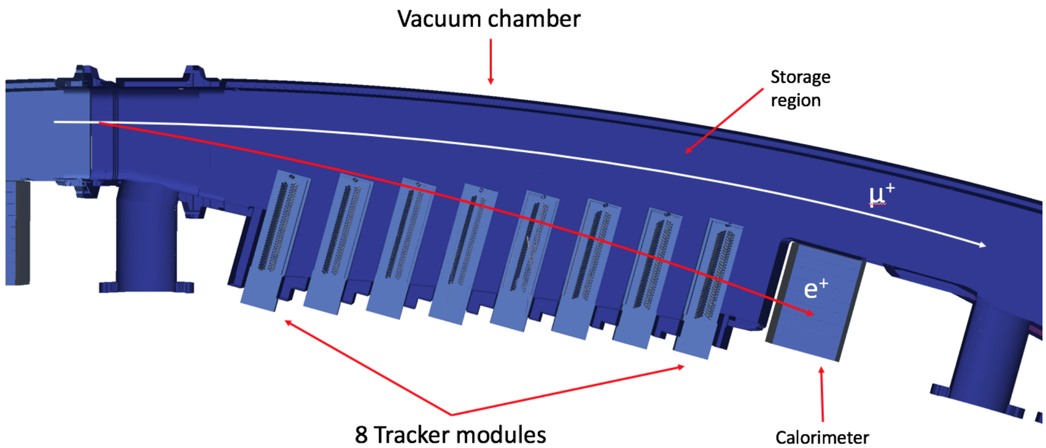

Figure 2·3: clean up and possibly replace

2.3 Detector Systems

2.3.1 Calorimeters

Electromagnetic calorimeters measure the times and energies of decay positrons as they curl inward from the storage region. There are 24 calorimeters located symmetrically around the inside of the ring in close proximity to the vacuum chamber, as shown in Figure ??. They lie close to the storage region in order to measure a large fraction of the total number of observable decay positrons, including the high energy decay positrons which curl inward only slightly more than the muons themselves do. Because they are in close proximity to the storage region and by extension the magnetic field, the calorimeters must be non-magnetic in order to avoid perturbing the magnetic field. Each calorimeter consists of 54 channels of PbF_2 crystals arrayed in a 6 high by 9 wide array, which measure Cerenkov light emitted by the impinging positrons as they pass through the crystals [7]. (Picture of single calo and its crystals here.) Each crystal is 2.5 x 2.5 x 14 cm^3. The light is read out by large area silicon photo-multiplier (SiPM) sensors.

In order to determine a_μ to the precision goal, there are modest requirements on the performance of the calorimeters. They must have a relative energy resolution of better than 5% at 2 GeV, in order for proper event selection [8]. They must have a timing resolution of better than 100 ps. The calorimeters must be able to resolve multiple incoming hits through temporal or spatial separation at 100% efficiency for time separations of greater than 5 ns in order to reduce the pileup systematic error due to the high rate. Finally, the gain of the measured hits must be stable to $< 0.1\%$ over a 200 μs time period within a fill, and unaffected by a pulse arriving in the same channel a few nanoseconds earlier. The long term gain stability over a time period of order seconds must be $< 1\%$.

(I've condensed quite a bit this section from the TDR - is that okay?)

To satisy these requirements SiPM sensors were chosen over PMTS...

and is wrapped in black Tedlar® foil

[11]

2.3.2 Laser System

For the gain, there is a laser system...

[2] [1] [3]

2.3.3 Template Fitting

2.3.4 Straw Trackers

The Muon $g - 2$ Experiment at Fermilab uses straw tracking detectors to measure decay positron trajectories for the purpose of determining the muon beam distribution and its characteristics (and other things....). By fitting these tracks and extrapolating back to the average decay point, the beam can be characterized in a non-destructive fashion. See section blah. This is important because of the need for matching the average observed magnetic field of the decaying muons and their resulting decay positron directions which result in the ω_a frequency.

The trackers are also useful for determining general beam diagnostics as well as the pitch correction and to a lesser extent the electric field correction (careful here). Cross-checking separately for pileup removal, hit verification, etc. is a powerful tool. Combining them in order to provide the muon distribution that the calorimeters directly see for the ω_a calculation is perhaps the most important role of the tracker. With three trackers, approximately 5% of decaying muons will result in measureable positron tracks assuming no pileup in the tracker, many of which do not hit the nearest calorimeter.

Each tracker module consists of 4 layers of 32 straws with a stereo angle of 7.5 degrees, the first two "U" layers oriented with the tops of the straws at a greater radial position, and the second two "V" layers oriented with the bottoms of the straws at a greater radial position. A tracking module is shown in Figure ??. There are 2 tracker stations located in front of calorimeters 13 and 19, or at approximately 180 and 270 degrees counting clockwise from the top most point of the ring where the inflector resides. Figure **??** shows this. (A third station sits empty after the inflector.) Each station consists of 8 tracking modules arranged in a staircase pattern that follows the curvature of the ring as seen in Figure ??.

In order to reduce the amount of multiple scattering within the straw tracking chambers as particles pass through them, the material of the straw trackers is minimized. Each straw is made of mylar foil, within which a 25 μm radius tungsten wire resides, and is filled with Argon-Ethane gas [**something**]. Fast moving particles ionize the gas as they pass through it, and the resulting ions are drawn to the wire which is held at high voltage. When they reach the wire (and the mylar) a signal can be read out which tells us that a particle was seen to pass through the straw. By combining many such signals in a brief time span, we are able to construct tracks of incident particles. (See section blah.) The resolution of hits within the straws is

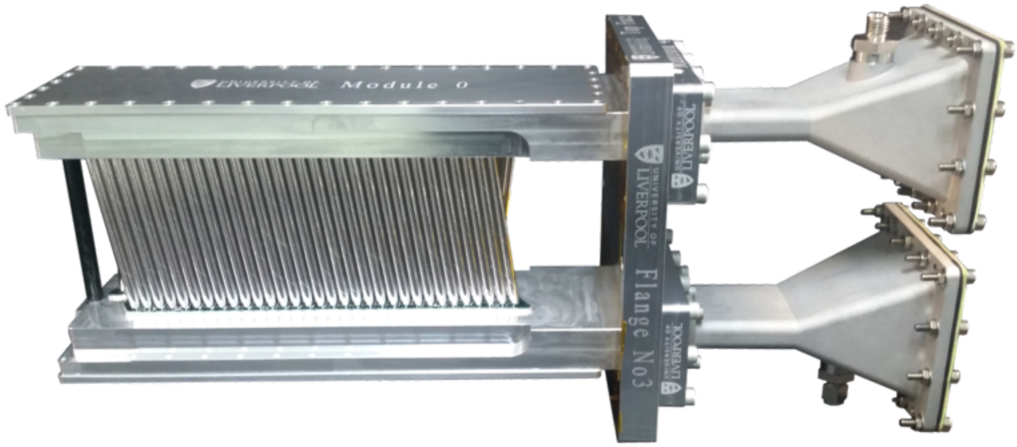

Figure 2·4: Shown is a picture of one of the many tracking modules used in the Muon $g-2$ experiment. The first layer of straws with a stereo angle of 7.5 degrees can be seen, with the other 3 straw layers hiding behind it. The beam direction is roughly into the page in this picture, to the left of the end of the module, and this view is what the decay positrons will see.

approximately 150 μm [**something**].

The signals of the straws are read out through...

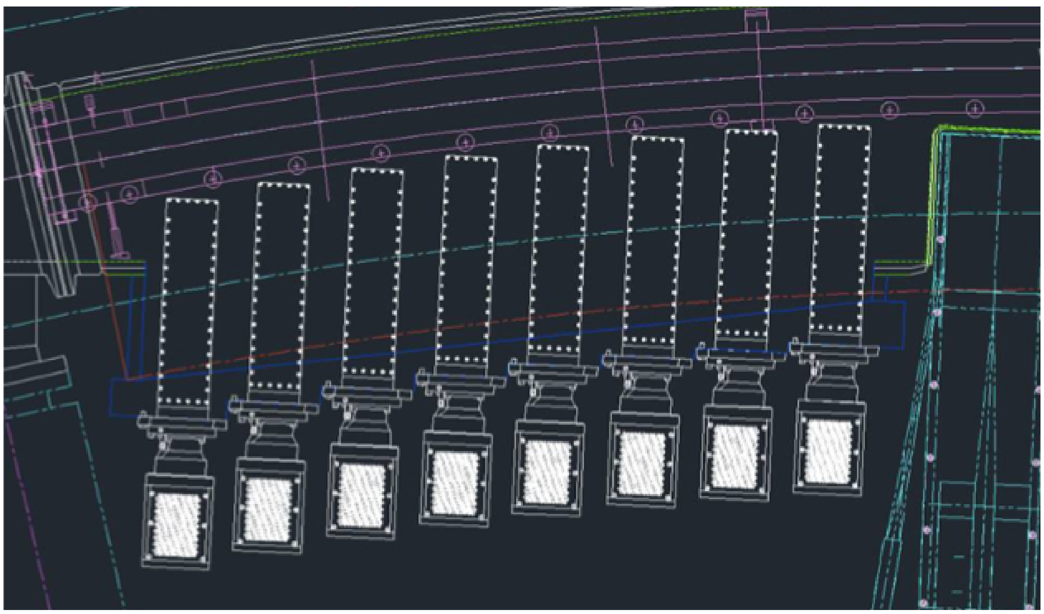

Figure 2·5: Tracker modules are arranged in the shown staircase pattern. In green and dark blue is the edge of the vacuum chamber (where the dark blue identifies the modification that was made to the old vacuum chambers), and it can be seen that vacuum chamber walls lie at the ends of the outside tracking modules. The position of a calorimeter can be seen in cyan at the right. The dark red spots are the locations of the outside magnet pole tips. From the shown geometry one can see that many positrons will hit either the tracker or the calorimeter but not both due to the acceptance differences.

Chapter 3

Magnetic Field Measurement

3.1 Trolley

3.2 Opera Simulations

Where does this section really go?

Chapter 4

Straw Tracking Analysis

4.1 Straw Tracking Intro

As was talked about briefly in section 2.3.4, the straw trackers are used to provide information about the muon beam, as well as info for the calorimeters. The straw track reconstruction is performed in several stages. The “Track Finding” stage takes incoming hits and decides which hits should be grouped together to form a single track for a single positron. The “Track Fitting” stage fits the measured positions of these invididivual hits and forms a single track describing the trajectory of the incident positron. Finally the “Track Extrapolation” stage takes the fitted track information and extrapolates the position and momentum components to the regions of interest, namely the storage region and the calorimeter.

-see the previous section for the hardware information... -Geane (Geometry and Error Propagation)

4.2 Track Finding

4.3 Track Fitting

The Geane fitting routines originated in Fortran with the EMC collaboration, and was used in the precursor E821 experiment as well as the PANDA experiment with some success [9], [13]. (I’m not actually aware of a useful reference for it’s use in E821, and there are some other instances of its use as well in other experiments. In E821

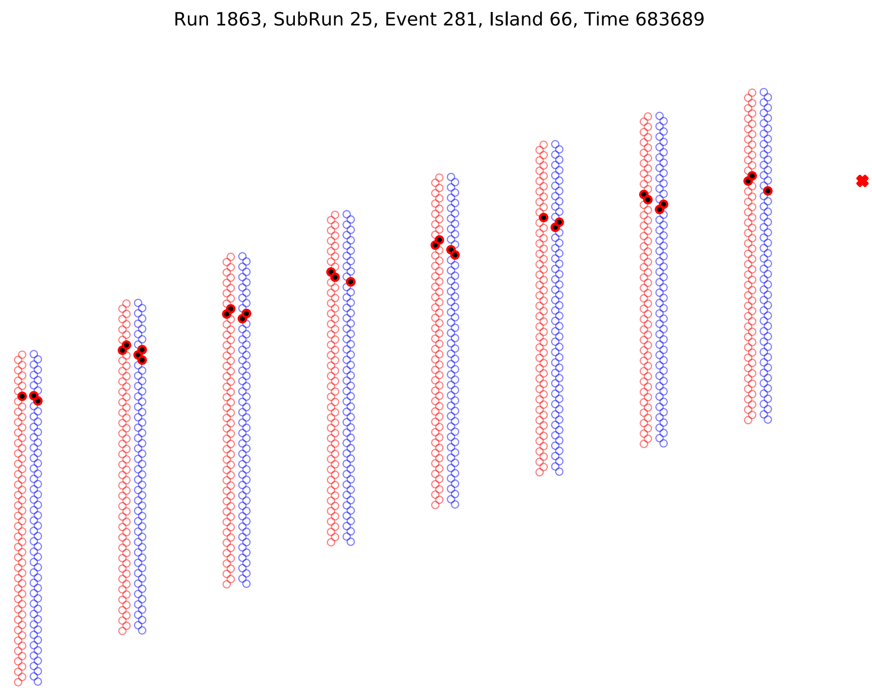

Figure 4·1: clean up and possibly replace

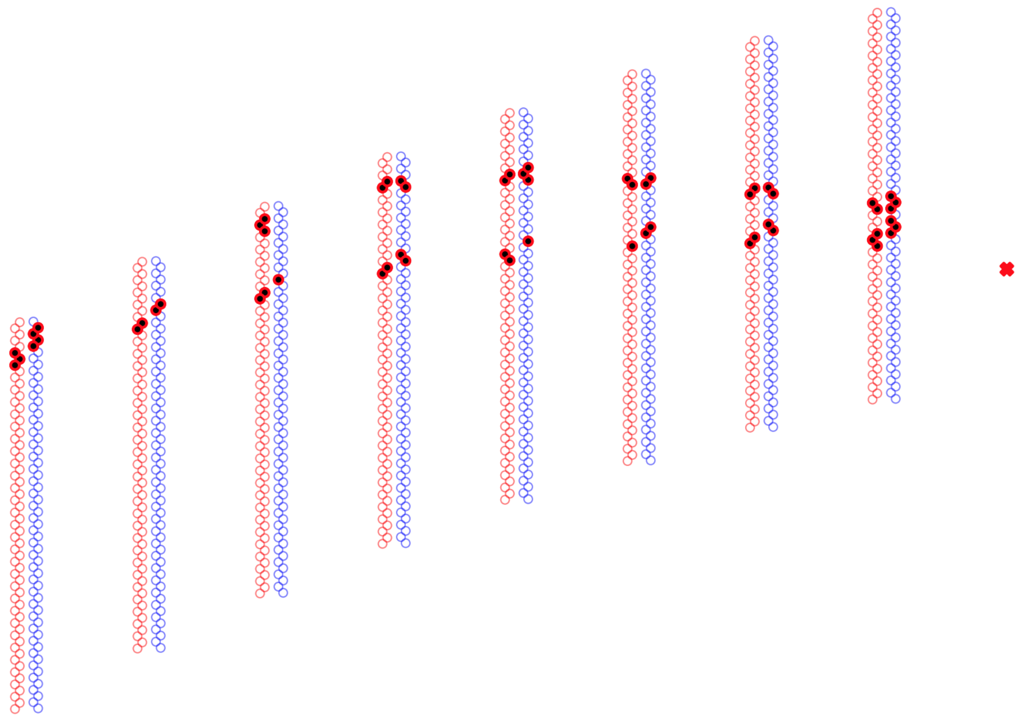

Figure 4·2: clean up and possibly replace

there was a single tracking chamber which was never put to full use.) The core error propagation routines were at some point added to Geant4 under the error_propagation directory which is included in all default installs. The tracking code strengths lie with its direct implementation and access to the Geant4 geometry and field, and its ability to handle the field inhomogeneties. The Geane fitting algorithm code which makes use of the Geant4 error propagation routines follows the structure of [9] and is detailed in the Formalism section in this paper. It is a relatively straight forward least squares global χ^2 minimization algorithm.

Because of the proximity of the trackers to the muon beam, they will lie within a region of varying magnetic field. The radial field of the trackers rises from 0 Tesla at the outer ends to roughly .3 Tesla at the inner top and bottom ends, and the vertical field drops approximately 50% from the storage dipole field of 1.451 Tesla. Shown in Figures ?? and ?? is the location of the tracker with respect to the horizontal

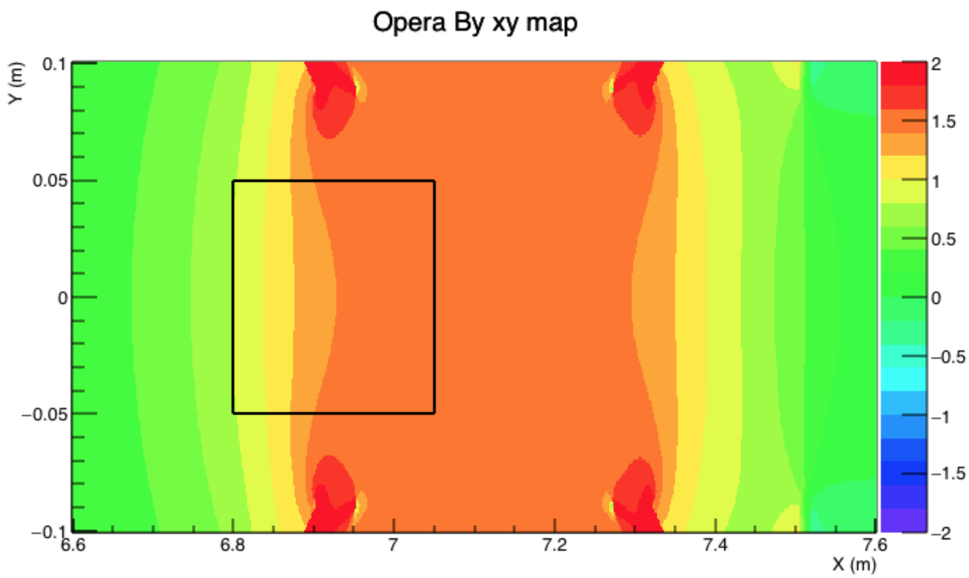

Figure 4·3: Shown is the vertical field of the $g-2$ magnet in and around the storage region as calculated in Opera 2D. The center of the storage region lies at 7.112 m along the x axis. The black box shows the rough location of the tracker with respect to the field (size exaggerated slightly). It can be seen that there is a large inhomogeneity within the tracker space, goring from left to right.

and vertical fields respectively. These large field gradients over the tracking detector region and the long extrapolation distance back to the muon decay point are special to Muon $g-2$. This is one of the main motivations for using the Geane fitting algorithm and routines, which has direct access to the field.

4.3.1 Track Fitting Formalism

I recommend reading [9], Chapter 4 of [13], and [10] in order to best understand the fitting algorithm. However, due to the at times confusing notation, ommitted equations or concepts, and differences between papers, I have attempted to summarize here the different sources and present the material in a more understandable and readable format. The implementation of the fitting algorithm into the code follows this section.

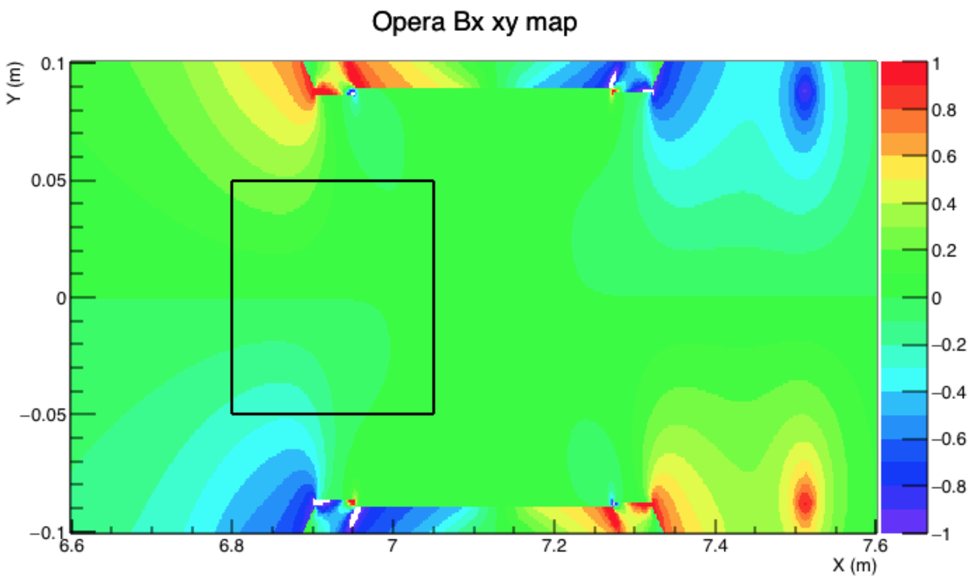

Figure 4·4: Shown is the radial field of the $g-2$ magnet in and around the storage region as calculated in Opera 2D. The center of the storage region lies at 7.112 m along the x axis. The black box shows the rough location of the tracker with respect to the field (size exaggerated slightly). It can be seen that there is a large homogeneity at the inner upper and lower ends compared to the right center. The shape of the pole pieces and tips can readily be seen.

One can define a χ^2 for a track in the usual way by dividing the residuals of measured and predicted track parameters by their errors:

$$\chi^2 = (\vec{p} - \vec{x})^T(\sigma^{-1})(\vec{p} - \vec{x}), \tag{4.1}$$

where $\vec{p}$ are predicted track parameters from a fit to the measured track parameters $\vec{x}$, and σ is a covariance matrix of errors on the fitted parameters. The Geant4 error propagation routines can be used to determine these predicted parameters and error matrices by propagating track parameters from some initial guesses. By minimizing this χ^2 with respect to the track parameters one can then fit and improve the track. The Geant4 error propagation routines propagate particles along their average trajectories neglecting the effects of discrete processes, using a helix equation along small enough steps where the change in the magnetic field is small. The predicted parameters are then a function of path length:

$$p_l = F_{l,l_0}(p_0), \tag{4.2}$$

where the path length can be defined how one wishes. In our system we have tracker planes defined at X positions, and limit path lengths to reach those planes. (From here on the dependence on path length or X position will be neglected, in favor of using plane indices.) In tandem, error matrices describing the expected distribution in true parameters about those predicted parameters due to said discrete process are also calculated:

$$\sigma^{ij} =< p^i p^j > - < p^i > \cdot < p^j >, \tag{4.3}$$

where i and j are track parameter indices. These parameter vectors are 5x1 objects defined in some track representation, as described in the Coordinate Systems section. The propagation of these parameters and error matrices are done using transport matrices, which express the infinitesimal changes in parameters at some plane (or path length) with respect to the parameters at some previous plane (or previous path length):

$$\delta p_N = T_{N,N-1}\delta p_{N-1}, \tag{4.4}$$

$$\sigma_N = T_{N,N-1}\sigma_{N-1}T^T_{N,N-1}. \tag{4.5}$$

Said transport and error matrices are 5x5 objects since the parameter vectors are 5x1 objects as described above. The calculation of these transport matrices, as well as details on the functional form of 4.2 are shown in [14].

With parameters defined on such planes, one can define the χ^2 as:

$$\chi^2 = \sum_{i=1}^{N}[(p_i(p) - x_i)^T(\sigma_i^{-1})(p_i(p) - x_i)], \tag{4.6}$$

where p_i are the average predicted parameters from some general starting parameters p. At first order one can solely include the measurement errors on parameters, which fill in the diagonals of σ_i, if random processes can be neglected. Unmeasured parameters should have measurement errors of infinity (or some large value) along the diagonals in the code, which account for the fact that residuals for unmeasured parameters do not exist. When the error matrix is inverted all rows and columns of the matrix with these large numbers will fall to 0 in the χ^2.

In order to get the best fit track, the χ^2 should be minimized with respect to the initial track parameters p, and evaluated at some chosen or fitted parameters:

$$\frac{\partial\chi^2}{\partial p}|_{p=p'_0} = 0, \tag{4.7}$$

resulting in

$$
\begin{aligned}
0 = \sum_{i=1}^{N} [(\frac{\partial p_i(p)}{\partial p} |_{p=p_0'})^T (\sigma_i^{-1}) (p_i(p_0') - x_i) \\
+ (p_i(p_0') - x_i)^T \frac{\partial(\sigma_i^{-1})}{\partial p} |_{p=p_0'} (p_i(p_0') - x_i) \\
+ (p_i(p_0') - x_i)^T (\sigma_i^{-1}) (\frac{\partial p_i(p)}{\partial p} |_{p=p_0'})]
\end{aligned}
\tag{4.8}
$$

where the 1st and 3rd terms are identical, and the 2nd term is small if one assumes that the error matrix doesn't change much with respect to the starting parameters. (Fair since most of the error comes from measurement, and as long as the initial guess is decent enough such that the path length through material doesn't change appreciably from one iteration to the next.) This simplifies to:

$$
\sum_{i=1}^{N} T_{i0}^T (\sigma_i^{-1}) (p_i(p_0') - x_i) = 0, \tag{4.9}
$$

which is just the top term with

$$
T_{i0} = \frac{\partial p_i(p)}{\partial p}. \tag{4.10}
$$

To solve this make the substitution

$$
p_i(p_0') = p_i(p_0) + \frac{\partial p_i(p_0)}{\partial p} \Delta p_0 = p_i(p_0) + T_{i0} \Delta p_0, \tag{4.11}
$$

where p_0' are the improved starting parameters for the next iteration calculated from the previous starting parameters p_0, and Δp_0 are the changes in the starting parameters to improve the track. This equation can be plugged into the above if one makes the assumption that T_{i0} does not change much from one iteration the next, which follows from the inherent nature of making small adjustments to the track in order to improve it.

After simplifying one arrives at

$$\Delta p_0 = \sigma_{p_0} \sum_{i=1}^{N} T_{i0}^T (\sigma_i^{-1})(x_i - p_i(p_0)), \tag{4.12}$$

where

$$\sigma_{p_0} = [\sum_{i=1}^{N} T_{i0}^T (\sigma_i^{-1}) T_{i0}]^{-1}, \tag{4.13}$$

is the 5x5 covariance matrix of fitted parameters on the starting plane, whose diagonals describe the errors in the 5 track parameters on that plane and in the region close to it. (The fit does not directly return fit errors for track parameters on other planes.) Δp_0 along with χ^2 is exactly what we want to determine since that is what allows us to fit and improve the track from iteration to iteration.

However, since random processes should not be neglected for optimal tracking results, it makes more sense to return to the original χ^2 in equation 4.1, only now the included matrix and vector objects are combined into one large linear algebra equation. Instead of a sum over N 5x1 objects multiplying 5x5 error matrices, the vectors are combined into a single 5Nx1 vector multiplying a single 5Nx5N matrix. The 5x5 diagonal blocks of this large error matrix should now include the effects due to material processes as calculated in Geant from equation 4.3 as well as the measurement errors.

Because now parameters at one plane are no longer independent of the parameters at other planes, due to correlations from these random processes, it's necessary to add off-diagonal elements into the large error matrix. These 5x5 blocks come from

$$\sigma_{MN} = T_{MN} \sigma_N, \tag{4.14}$$

for the top diagonals, and the transpose for the bottom diagaonals, where M and N are two separate planes within the detector. (σ_N is the error matrix on plane N calculated from the starting plane.) This follows from equation 4.3 evaluated at plane M with respect to a path length from plane N, and not plane 0, which is equivalent to 4.14.

You can then minimize the χ^2 in the same way, only again with the matrix objects being aggregates of the per plane objects:

$$\Delta\vec{p}_0 = \sigma_{p_0}\tau^T\sigma^{-1}(\vec{x} - \vec{p}), \tag{4.15}$$

$$\sigma_{p_0} = [\tau^T\sigma^{-1}\tau]^{-1}, \tag{4.16}$$

where τ is the combined transport matrices from the individual 5x5 matrices, a 5Nx5 object.

The unmeasured parameter errors of infinity still come into play in the final calculation in the same was as before. Because however these matrix objects are very large, and the tracking must have a certain amount of speed in order to keep up with data, it is useful to reduce the size of these matrices. (It also makes things easier programming wise. Note that there are other some other ways to speed things up, specifically the banded inversion method as described in reference [10]. This method was not used in favor of getting the code working in the simpler form in the first place, but it is a possiblity in the future to use this technique to speed things up even more.) It suffices to simply remove all rows and columns where said infinity values exist in the error matrix. This is mathematically equivalent to inverting the error matrix with the infinities included, which make all rows and columns where they exist go to zero. The associated unmeasured parameter rows in the residual vector and transport matrices must similarly be removed. This results in an Nx1 residual vector, NxN error matrix, 5xN combined transport matrix transpose, which multiply against the 5x5 covariance matrix out front to still result in a 5x1 fix to the starting parameters, and a scalar χ^2 value. (Note that these element removals should be done just before the final calculation, and not higher up in the algrebra, otherwise plane correlations are not properly calculated.)

By calculating the last two equations one can fit the track, acquire a χ^2 describing the degree of the fit, determine how the track parameters can be improved at the starting point, and calculate errors on those starting parameters. This algorithm can be iterated a number of times to get a best fit track until successive iterations produce no improvement, where usually 3 or 4 iterations is enough. Note that there is remarkable robustness with respect to the initial starting parameters in fitting the track. Of course if the initial starting paramaters are too poor, then the fit will not converge. All of these calculations are completed within the GeaneFitter.cc file within the framework.

4.4 Track Extrapolation

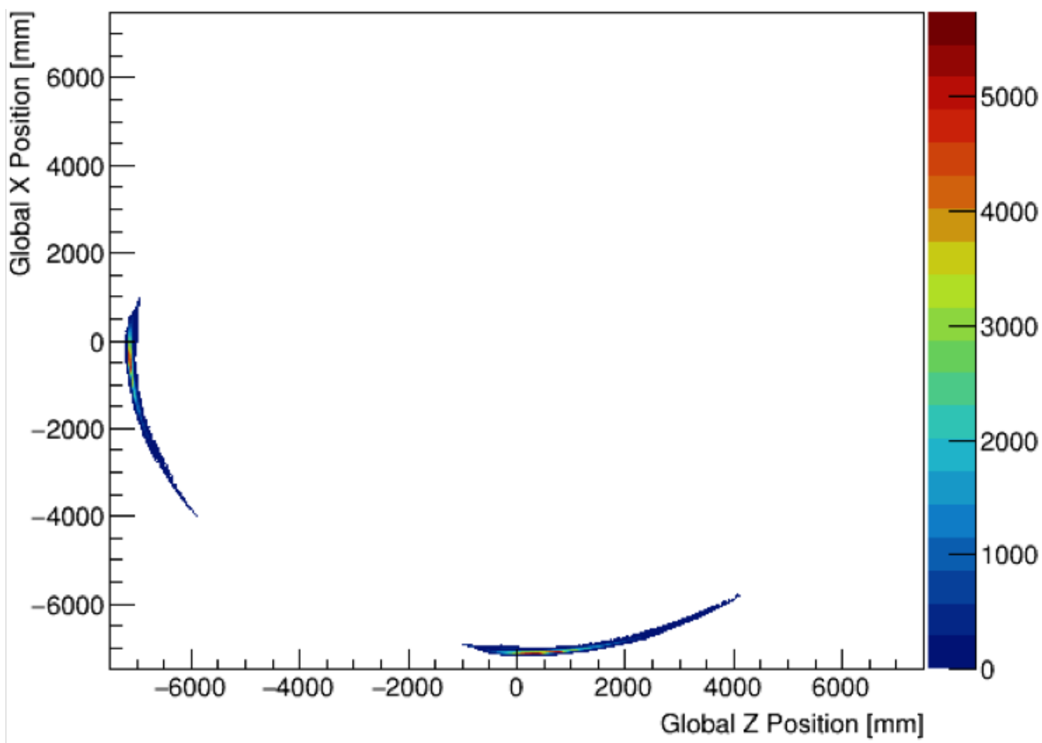

Figure 4·5: preliminary replace at some point

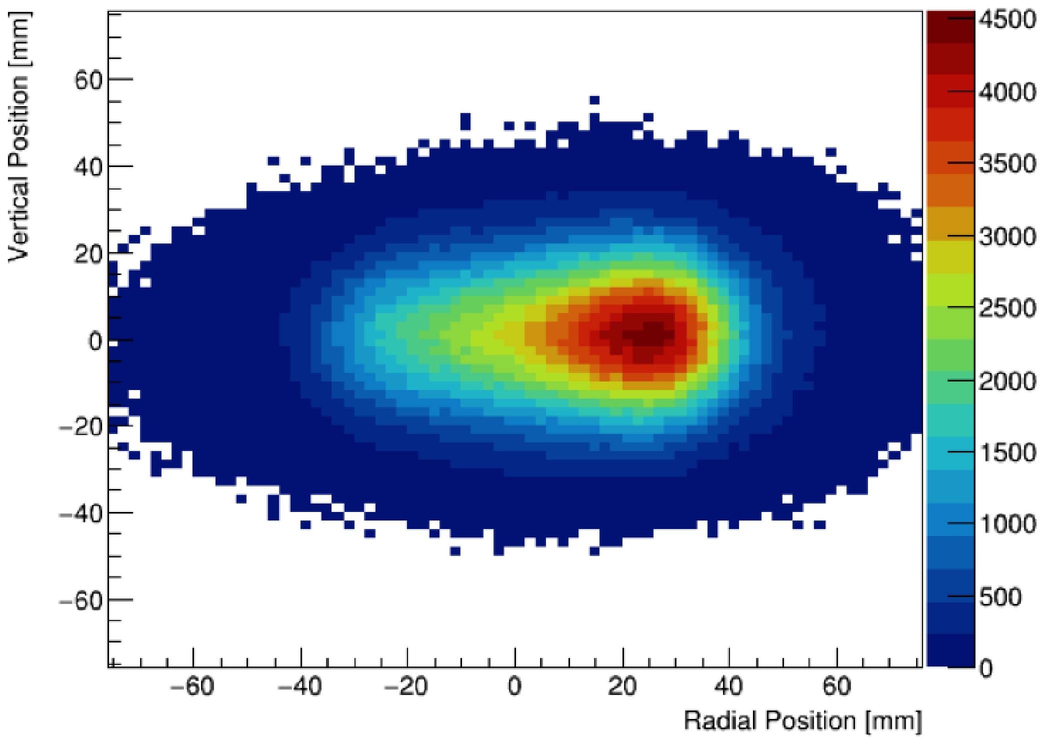

Figure 4·6: preliminary replace at some point

Chapter 5

ω_a Measurement

5.1 Data

5.2 Spectra Making

5.2.1 Clustering

5.2.2 Histogramming

5.3 Fitting

5.4 Systematic Errors

Chapter 6

Conclusion

6.1 Final Value

test4

Appendix A

Proof of xyz

This is the appendix.

Bibliography

[1] A. Anastasi et al. “Electron beam test of key elements of the laser-based calibration system for the muon $g-2$ experiment”. In: *Nucl. Instrum. Meth.* A842 (2017), pp. 86–91. DOI: 10.1016/j.nima.2016.10.047. arXiv: 1610.03210 [physics.ins-det].

[2] A. Anastasi et al. “Test of candidate light distributors for the muon $(g-2)$ laser calibration system”. In: *Nucl. Instrum. Meth.* A788 (2015), pp. 43–48. DOI: 10.1016/j.nima.2015.03.071. arXiv: 1504.00132 [physics.ins-det].

[3] A. Anastasi et al. “The laser control of the muon $g-2$ experiment at Fermilab”. In: *JINST* 13.02 (2018), T02009. DOI: 10.1088/1748-0221/13/02/T02009.

[4] G. W. Bennett et al. “Final Report of the Muon E821 Anomalous Magnetic Moment Measurement at BNL”. In: *Phys. Rev.* D73 (2006), p. 072003. DOI: 10.1103/PhysRevD.73.072003. arXiv: hep-ex/0602035 [hep-ex].

[5] Max Dohse. “TikZ-FeynHand: Basic User Guide”. In: (2018). arXiv: 1802.00689 [cs.OH].

[6] Joshua Ellis. “TikZ-Feynman: Feynman diagrams with TikZ”. In: *Comput. Phys. Commun.* 210 (2017), pp. 103–123. DOI: 10.1016/j.cpc.2016.08.019. arXiv: 1601.05437 [hep-ph].

[7] A. T. Fienberg et al. “Studies of an array of PbF_2 Cherenkov crystals with large-area SiPM readout”. In: *Nucl. Instrum. Meth.* A783 (2015), pp. 12–21. DOI: 10.1016/j.nima.2015.02.028. arXiv: 1412.5525 [physics.ins-det].

[8] J. Grange et al. “Muon (g-2) Technical Design Report”. In: (2015). arXiv: 1501.06858 [physics.ins-det].

[9] V. Innocente, M. Maire, and E. Nagy. “GEANE: Average tracking and error propagation package”. In: *MC 91: Detector and event simulation in high-energy physics. Proceedings, Workshop, Amsterdam, Netherlands, April 8-12, 1991.* 1991, pp. 58–78. URL: http://innocentonnice.web.cern.ch/innocentonnice/napoli99/geane_manual.ps.

[10] V. Innocente and E. Nagy. “Trajectory fit in presence of dense materials”. In: *Nucl. Instrum. Meth.* A324 (1993), pp. 297–306. DOI: 10.1016/0168-9002(93)90992-Q.

[11] J. Kaspar et al. “Design and performance of SiPM-based readout of PbF_2 crystals for high-rate, precision timing applications”. In: *JINST* 12.01 (2017), P01009. DOI: 10.1088/1748-0221/12/01/P01009. arXiv: 1611.03180 [physics.ins-det].

[12] Alexander Keshavarzi, Daisuke Nomura, and Thomas Teubner. “Muon $g-2$ and $\alpha(M_Z^2)$: a new data-based analysis”. In: *Phys. Rev.* D97.11 (2018), p. 114025. DOI: 10.1103/PhysRevD.97.114025. arXiv: 1802.02995 [hep-ph].

[13] Lia Lavezzi. “The fit of nuclear tracks in high precision spectroscopy experiments”. pp. 57-86. PhD thesis. Pavia U., 2007. URL: http://bamboo.pv.infn.it/doc/L_Lavezzi.pdf.

[14] A. Strandlie and W. Wittek. “Derivation of Jacobians for the propagation of covariance matrices of track parameters in homogeneous magnetic fields”. In: *Nucl. Instrum. Meth.* A566 (2006), pp. 687–698.

[15] Diktys Stratakis et al. “Accelerator performance analysis of the Fermilab Muon Campus”. In: *Phys. Rev. Accel. Beams* 20.11 (2017), p. 111003. DOI: 10.1103/PhysRevAccelBeams.20.111003. arXiv: 1803.00597 [physics.acc-ph].

CURRICULUM VITAE

Joe Graduate

Basically, this needs to be worked out by each individual, however the same format, margins, typeface, and type size must be used as in the rest of the dissertation.